IEPC-95-111

Six-Color Video Pyrometry with Application to MPD Thrusters *

Edgar Y. Choueiri†, Vincent Chiravalle‡, George E. Miller§
& Robert G. Jahn¶
Electric Propulsion and Plasma Dynamics Laboratory (EPPDyL)
Princeton University, Princeton NJ 08544.

IEPC-95-111‖

This work is dedicated to Woldemar F. von Jaskowsky on his eighteith birthday.

Abstract

A six-color video pyrometer (SCVP) that exploits the advantages of computer aided video analysis was developed for spatially resolved high temperature measurements of surfaces of unknown emissivity. The SCVP is an accurate and relatively inexpensive tool for high-temperature pyrometry developed by mechanically and electronically altering an off-the-shelf CCD camera and by using computer algorithms for image processing and statistical analysis. The camera alterations allow video taping of images at 30 fps in full synchronicity with a wheel spinning in front of the array and carrying six judiciously chosen narrow bandwidth optical filters. This results in a time resolution of 200 ms and an arbitrary spatial resolution proportional to the number of pixels over which the object is focused. Through a multiple regression analysis on a set of 15 coupled pyrometric equations for each pixel, an estimate of the true temperature and the associated variance can be obtained. Calibration of the SCVP using a standard lamp and a 655 nm pyrometer resulted in an error well below 10% in the true temperature measurement (which ranged between 1750 and 2000 °K) of an MPD thruster cathode. The SCVP is intended for use on lithium-fed MPD thruster components whose emissivity is largely unknown.

*This work is supported by Thermacore Inc. through an SBIR contract from NASA-JPL.

†Chief Scientist and Lab. Manager. Member AIAA.

‡Student supported by the New Jersey NASA Space Grant Consortium.

§System Engineer, EPPDyL.

¶Professor of Aerospace Sciences.

‖Presented at the 24th Electric Propulsion Conference.

1 Introduction

The optical measurement of the temperature of a surface that is hot enough to emit radiation detectable by a light intensity meter is simple when the emissivity of that surface is known. Commercially available pyrometers, operating at a fixed wavelength, are commonly used in high temperature situations where thermocouples are not viable. The governing equation for these instruments, operating at optical wavelengths within Wien's approximation, is the fundamental pyrometric relation

$$T = \left(\frac{1}{T_B} + \frac{\lambda \ln \epsilon}{C} \right)^{-1}, \qquad (1)$$

where T is the true temperature, T_B the brightness temperature, ϵ the emissivity, C the fundamental radiation constant and λ the wavelength at which the brightness temperature is measured. The brightness temperature is defined as the temperature of a blackbody that emits the same amount of radiation, at wavelength λ, as the surface in question.

In some situations an accurate knowledge of the emissivity may not be available. Such is the case of the lithium-fed magnetoplasmadynamic (MPD) thruster currently being studied at our laboratory. The components of the thruster may or may not be covered with lithium whose emissivity is unknown. An accurate high temperature diagnostic is needed to assess the effect of lithium on lowering the effective cathode temperature which controls the evaporative erosion rate of the cathode.

Devices are available to infer emissivity by measuring the reflectance of polarized light from a surface as discussed in Ref. [1]. These instruments, however, are expensive and of limited applicability when considering metallic surfaces with high reflectivity.

When the emissivity is uncertain, one-color pyrometry at high temperature can incur errors that are too large to be tolerated. An improvement on the single-color pyrometer in these situations, can be achieved by carrying the measurements at two distinct wavelengths. In the simplest case, one may assume that the wavelengths are close enough and neglect the change in the emissivity (or in $\ln\epsilon$) over that range. Under this assumption, Eq. (1) yields

$$T = \frac{1-\Lambda}{\frac{1}{T_{B1}} - \frac{\Lambda}{T_{B2}}}, \tag{2}$$

where $\Lambda \equiv \lambda_1/\lambda_2$ and the subscripts refer to conditions at the two distinct wavelengths. This provides an estimate of the true temperature without knowing the emissivity. The application and limitation of the two-color pyrometer are discussed in Refs. [2] and [3]. The assumption underlying two-color pyrometry can be shown to lead to unacceptable errors[4] in many practical applications including our particular case concerning the MPD thruster.

An extension of this idea to multiple wavelength has been elaborated during the past two decades[5, 6, 7, 8]. This generally requires the assumption that $\ln\epsilon$ is a smooth function of wavelength, i.e. the following equation holds

$$\ln\epsilon = \sum_i a_i \lambda^i, \tag{3}$$

where the coefficients a_i are unknown functions of temperature. Various statistical schemes have been proposed to reduce the data and minimize errors. A recent method (1992) developed by Hoch[8] is the most sophisticated to date and was proven to yield high accuracy measurements.

Multi-color pyrometers reported in the literature, such as those described in Refs. [6] and [7], use six wavelengths and an array of photodiodes as light detectors. These instruments are good for localized measurements and are not particularly useful for our application where a spatially resolved temperature picture is sought.

By combining the features of CCD video, computer-aided image processing, and recently developed statistical schemes for multi-wavelength pyrometry, we have developed a six-color video pyrometer (SCVP) that allows temperature measurement in the 1600-2800 °K range, with acceptable accuracy, high spatial resolution and a temporal resolution of 200 ms.

This paper describes critical issues associated with the design, development and implementation of the SCVP. These include, the mechanical and electronic alterations made on the CCD camera, the selection of the bandwidth filters, the selection of the appropriate slit size for the filter aperture silts that prevent mixing of images at different wavelengths, the application of neutral density compensation to avoid camera saturation, and the adjustment of the voltage output of the SCVP to achieve maximum light intensity resolution. The calibration procedure is described and expressions for the uncertainties are given. The data reduction algorithm that allows the true temperature and associated variances to be estimated for each pixel is also described. Finally, a demonstration of the capability of the pyrometer is made by measuring the cathode temperature of a steady-state 20-kW level MPD thruster.

2 SCVP System Description

2.1 SCVP Components

The SCVP consists of six components: a Video Logic Instar CDR-460 CCD camera combined with a Vivitar 70-300 mm zoom lens which measures light intensity, a filter wheel, containing six 3 nm bandwidth filters, an electric motor coupled to a control circuit that keeps the filter wheel rotating in phase with the video frame transmission, a slit wheel, with six aperture slits for the bandwidth filters, a video frame marking circuit for frame synchronized labelling and a saturation alarm circuit that warns when neutral density compensation is needed to keep the camera from saturating.

The wavelengths of the filters were selected to minimize the interference of argon and lithium plasma emission. The wavelengths are 500 nm, 532.4 nm, 568 nm, 600 nm, 632.8 nm, and 660 nm. The selection of these filters is discussed in Section 2.2.4.

The video frame marker circuit, custom-altered by American Video Equipment, adds a digital counter to each frame of the video output. A small magnet was placed on the shaft to trigger a Hall sensor that increments the counter every time the 500 nm bandwidth filter passes in front of the CCD array. The alarm circuit activates a photodiode when the video output voltage of the camera is near the level corresponding to the saturation state of the CCD array.

Details on these components are given in the following sections. A schematic of the SCVP is shown in Fig. (1).

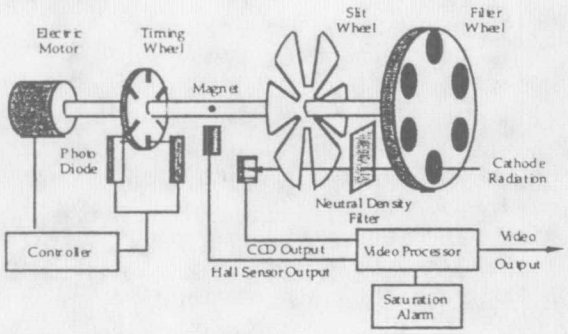

Figure 1: SCVP Schematic.

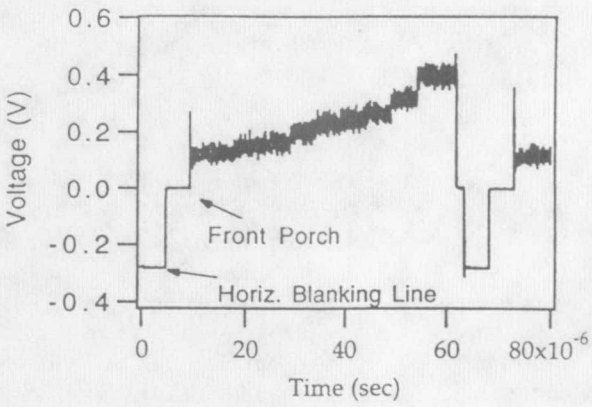

Figure 2: A line of standard video.

2.2 SCVP Design and Development Issues

2.2.1 Analog Video Output

We selected a CCD camera with an analog output since such cameras are considerably less expensive than those with digital output. The main disadvantage of such a camera is the susceptibility of the pixel values to noise from the analog transmission line. This problem was dealt with using a digital filter on the digitized data as described in Section 4.2.

The video output of the SCVP is formatted according to the standard established by the National Television Systems Committee (NTSC), so that each frame contains a total of 525 lines generated from the interlacing of two fields, each with half the number of lines. A line of video in NTSC format is shown in Fig. 2, and two plateaus are highlighted, the horizontal blanking line and the "front porch".

The horizontal blanking line marks the beginning of a video line. Convention dictates that the voltage value for each pixel, V_s, is measured relative to the front porch. The voltage difference between the horizontal blanking line and the front porch, V_s, is a characteristic of the camera, and is used to convert the voltage value of a pixel into information about light intensity.

Video from the SCVP is recorded in S-Video format on a Panasonic AG-1960 ProLine video tape recorder, using Maxwell XR-S120 video tape. Pixel intensities are obtained in the form of non-dimensional grey level units (0-255) that are extracted from the video tape, one field at at time, using a Macintosh IIfx computer with a 32-bit digitizing video board (Raster Ops 364) operating in 8-bit mode. The conversion is given by

$$G_L = 255 - \frac{100 - 40\frac{V_p}{V_s}}{92.5}, \qquad (4)$$

where G_L denotes the pixel intensity in greyscale units. When looking at a monitor, a pixel with zero grey level appears as black and a pixel with a grey level value of 255 appears white. As the white threshold is surpassed the voltage output of the camera reaches a peak due to charge saturation of the CCD array. Any voltage above the white threshold is assigned a value of 255 by the digitizing board.

2.2.2 Bandwidth Adjustment

The saturation state of the SCVP was studied by removing the lens mount, the filter wheel and the metal case so that the CCD array was completely exposed to the fluorescent light in the laboratory. Measurements of the video output voltage were made using a 320 Nicolet Digital Oscilloscope attached to a 75 Ω terminator. A constant voltage peak was observed on all the lines, confirming that saturation was occurring. The grey level calculated from this voltage, however, was only 200 units, significantly below the white threshold. This would cause a decrease in the effective resolution of the SCVP. In order to improve the pixel resolution, the V_s of the SCVP was decreased by turning a pin on the circuit board until

the saturation point of the CCD array was above 255 grey level units.

2.2.3 Filter Wheel Addition and Synchronization

The rate of video frame production from the SCVP follows the NTSC convention of 30 frames per second. Originally the Video Logic camera had a wheel with a single slit that rotated at 1800 RPM in front of the CCD array, performing the role of a mechanical shutter. A control circuit synchronized the frame transmission rate of the camera with the aperture slit rotation rate, so that a frame exposure occurred while the slit was in front of the CCD array. The control circuit receives as input a signal from the camera that marks the beginning of a frame and a signal from a photodiode that marks the time when light from an opposing diode passes through a slit on a timing wheel connected to the shaft. The photodiodes and the timing wheel are shown in Fig. 1. The voltage supplied to the 12 V motor that turns the shaft is adjusted by the control circuit until its two input signals are in phase. Before modifications were made to the camera to make the SCVP the timing wheel had only one slit that was aligned with the slit on the shutter wheel.

The shutter wheel was replaced with the filter wheel shown in Fig. 1. Five more slits were added to the timing wheel, each one aligned with a filter on the filter wheel. The control circuit maintains the shaft rotation rate at 300 RPM after start-up, thus allowing allows six frames to be taken during one revolution of the wheel. A set of reduction gears was added to the motor to allow a more efficient transfer of power to the shaft at this lower rotation rate.

2.2.4 Filter Selection

The CCD camera is sensitive to wavelengths from approximately 450 nm to 1100 nm. Anything outside of that region might not register with enough intensity to be useful for analysis. Moreover, it is preferable to chose larger wavelengths because the radiant intensity will be greater and thus lower temperatures will be imaged more accurately[9].

With the above considerations in mind, checks were made for both argon and lithium emission lines using data from ref. [10] and ref. [11] with the intent to exclude filters with wavelengths coinciding with line emission from the plasma. While argon has many emission lines, lithium has only two of any concern. It is necessary to avoid some strong lithium emission lines at 548.5 nm, 610.4 nm and 670.8 nm. For argon a table of emission lines and their intensities, over the camera's wavelength range, was created in Excel 4.0 to aide in the filter selection process.

With this table and a list of filters available from a given manufacturer, the total amount of radiant intensity captured by each filter could easily be tabulated. For instance, we generated a table for the interference filters produced by Corion. It then became clear which filters would be effective in blocking out background plasma radiation and which ones would not. Considering the spectral response of our CCD camera and the impossibility to operate in the infrared, because of the smearing problem (which led to the use of a Corion complete infra-red suppressor FR-400-R with 70% average transmittance from 400 nm to 650 nm), it was decided that the best wavelength range was that between approximately 500 nm and 650 nm. In order to keep errors low within this range, the filters should be more or less equally spaced. From this information the following filter combination was chosen: 500 nm, 532.4 nm, 568 nm, 600 nm, 632.8 nm, and 660 nm.

One concern about using filters with a bandwidth of 10 nm was the errors they might introduce. In the data analysis, it is commonly assumed that the bandwidth is small so that no additional uncertainties are introduced. However, Coates[12] showed that as long as the transmission curves of the filters are known, the wavelengths can be corrected. In ref. [12] he outlines a number of different methods of varying effectiveness for accomplishing this task, all involving a numerical integration of the filter's transmission curve. Coates' method, though quite involved, reduces the error to an acceptable amount even for filters with seemingly inappropriate transmission characteristics. A better solution is to use filters with smaller bandwidths, which has the twofold advantage of not only reducing the error due to the bandwidth but also filtering out more of the background plasma radiation. For this reason all filters used had 3 nm bandwidth.

The choice of the 632.8 nm filter allows a He/Ne Laser light to be used as a spot marker on the object in order to focus the camera prior to the experiment.

2.2.5 Aperature Slits

The size of aperture slits controls the exposure time of the CCD array to each filter. The CCD array discharges every 1/60 sec and two CCD discharges produce one video frame with total exposure of 1/30 sec. For six-color pyrometry to work each of the six frames

captured as the filter wheel completes one rotation must be an exposure of only one of the filters. Experiments were performed, using the SCVP and an incandescent light source, to determine the maximum slit size that would produce an image of a filter in only one frame. Five of the six filters on the wheel were covered, and slits of various sizes were used to mask part of the exposed filter. The maximum slit size was fixed at 12 degrees of arc relative to the filter wheel.

The aperture slit wheel, shown in Fig. 1, was manufactured from aluminum stock using a Bridgeport computerized milling machine. The largest slit of 12 degrees was used for the 500 nm and 532.4 nm filters since the emission of a blackbody at 2500 °K at these wavelengths is less than the emission at higher wavelengths. The spectral emission of a blackbody at different temperatures in shown in Fig. 3. For the 660 nm and 632.8 nm filters 4 degree slit sizes were used and 8 degree slits were chosen for the middle wavelengths, 600 nm and 568 nm. It was hoped that this selection of slit sizes for the filters would prevent the CCD array from saturating during SCVP operation, without the need for neutral density compensation.

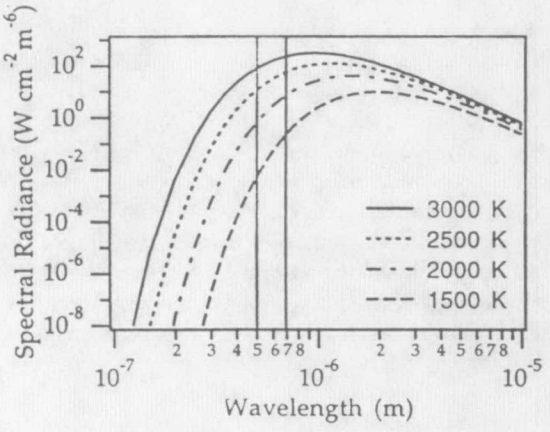

Figure 3: Spectral radiance of a blackbody in temperature of interest to MPD thrusters.

2.2.6 Neutral Density Compensation

Tests were performed using a General Electric Projection Lamp (18A/2P/T10) with a tungsten filament, to determine whether neutral density compensation would be required to avoid saturation when observing an MPD thruster cathode. Brightness temperature measurements of the lamp were made over the current range, 9.4 to 18 A, using a Leeds & Northrup Optical Pyrometer (Cat. No. 9622-0, Serial No. 704529) operating at 655 nm. Details concerning the operation of vanishing filament pyrometers are discussed in Ref. [13]. The pyrometer was recalibrated at the National Institute of Standards, and Eq. 5 gives the correction factor, P_c, applied to a measurement made with the pyrometer, T_{Bm}, to obtain the true brightness temperature.

$$P_c = 1.008 - 1.8306e^{-5}\, T_{Bm} + 9.6192e^{-9}\, T_{Bm}^2. \quad (5)$$

Five T_{Bm} measurements were taken at each current value, from which an average and standard deviation were obtained. The correction factor was then applied to the average and error propagation analysis was performed to compute a weight for each measurement.

An analytic function of current, I, with parameters A and B, shown below, was fitted to this reduced data, using a least squares algorithm.

$$T_B = A + B\sqrt{I} \quad (6)$$

The dependence of T_B on the $\sqrt{I}$ term follows from making the approximation that the lamp radiates as a blackbody and that its electric properties are given by Ohm's law. The resulting fit and the data set are presented in Fig. 4.

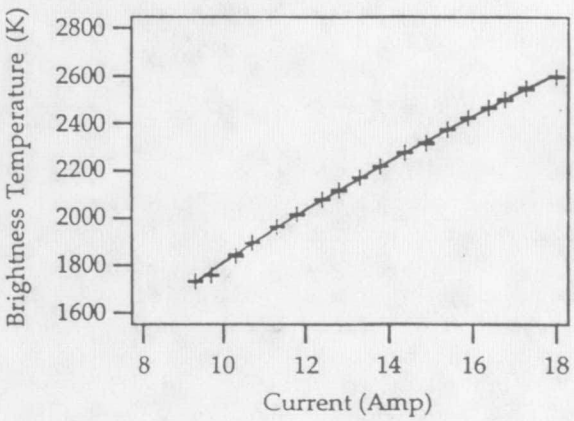

Figure 4: Brightness temperature data at 655 nm for the tungsten source.

The lamp was placed in the Steady-State Low-Power Facility at EPPDyL, in the same location where the MPD thruster would be mounted during

experiments. The SCVP was focused on the tungsten filament, with the lens aperture set at f-11. The position of the lamp and the SCVP are shown in Fig. 5. The current of the lamp was adjusted during the experiment to simulate the light intensities that would be encountered when observing MPD electrodes operation. The voltage output of the SCVP was observed on an oscilloscope to observe if saturation was occurring. Taking the lamp brightness temperature at 655 nm as an approximation to the true temperature of the filament, the 660 nm filter and the 600 nm filter began to saturate the SCVP at 2000 °K. At 2200 °K all the filters saturated the SCVP. It was evident that neutral density compensation would be required for the SCVP to measure temperatures around 2500 °K. Because some of the filters caused saturation at lower temperatures relative to the others, two approaches were taken in applying neutral density compensation. Wratten neutral density filters (No.96, N.D. 0.3), cut in rectangular pieces were inserted between the slit wheel and the filter to cover three of the filters. The 660 nm filter was covered with two neutral density filters and both the 600 nm and 532 nm filters were covered with one. Subsequent tests confirmed that the addition of these neutral density filters prevented SCVP saturation below 2200 °K. A single Wratten neutral density filter (No. 96, N.D. 1.0) was placed in front of the lens when the lamp was above 2200 °K. This compensation allowed the lamp to be observed at brightness temperatures of 2600 °K ($\lambda = 655\ nm$) without saturation. The lowest temperature that can be measured by this implementation of the SCVP is around 1750 °K.

3 Calibration Procedure

The SCVP produces six video frames of its object, one at each of the six wavelengths. Light intensity information for the pixels that comprise a frame is extracted in the form of grey level units. The grey level value for each pixel is then converted into a brightness temperature at the appropriate wavelength. A single point on the surface, therefore, has six brightness temperatures associated with it, one for each wavelength. The six brightness temperatures are used in a statistical algorithm, as described in Section 4, to determine the true temperature at that point on the surface. A calibration was performed to relate grey level to brightness temperature for each wavelength and for two different conditions, one where a neutral density filter was placed in front of the lens, and one where the lens was bare.

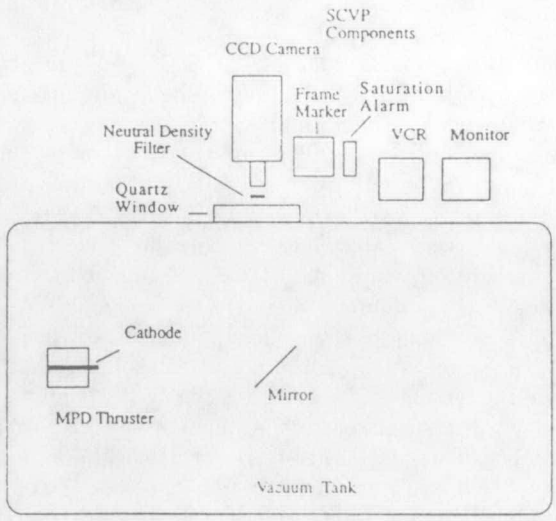

Figure 5: SCVP set-up in the Steady-State Low Power (SSLP) Facility.

3.1 Lamp Current to Brightness Temperature

The first step in the calibration process involved determining six functions, one for each wavelength, that relate lamp current to brightness temperature. This was accomplished by reducing the data of the lamp brightness temperature at 655 nm, mentioned previously, to get a single function pairing lamp current to true temperature. The true temperature was obtained by iteratively solving Eq. 1 using a temperature dependent expression for the emissivity of tungsten, derived from the experimental data of Larrabee[14]. The function for the emissivity is given below and it is accurate to within 0.5%.

$$\epsilon = 0.4655 + 0.01558\lambda + 2.675 \times 10^{-5} T - 7.305 \times 10^{-5} \lambda T \quad (7)$$

An estimate of the uncertainty in the true temperature was made due to the uncertainties in the brightness temperature and in the emissivity, following methods outlined in Ref. [15]. The calculated uncertainty in any one of the true temperature values was no greater than 0.3% or 6 °K. The reduced data was fitted to a function with the form of Eq. 6 and the result is shown in Fig. 6.

Having obtained the true temperature, Eq. 1 was used together with Eq. 7 to calculate the brightness temperature and its uncertainty at each of the six

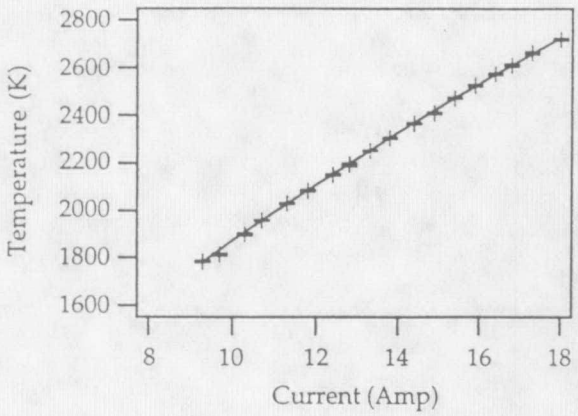

Figure 6: True temperature of the tungsten source.

wavelengths. These six sets of data points were then fitted using Eq. 6, and the variances and covariance of the coefficients, A and B were determined for later use in estimating the error in the calibration.

3.2 Brightness Temperature versus Grey Level

After the six functions relating brightness temperature to current were computed, additional functions were determined relating the grey level of the lamp to the lamp current, using the SCVP. With the lamp placed in the vacuum tank as shown in Fig. 5, video was taken of the lamp at different current levels ranging from 9.3 to 12.8 A, with the lens aperture set at f-11. The grey level values of a rectangular strip, 3 by 40 pixels, in the center of the tungsten filament were extracted from the video frames. An average and a weight were computed for the grey level of the lamp at each value of current. The data was fit to a straight line, $C + D \times I$, where C and D are parameters and I is the current. Six functions were obtained in this way, one for each wavelength, and the variances of the coefficients, C and D were computed to estimate the final error in the calibration.

The same procedure was repeated to find six relations for grey level versus current, when the lamp current ranged from 13 to 18 A, but this time a neutral density filter (No. 96, N.D. 1.0) was placed in front of the SCVP. Thus two sets of six functions were obtained, one set that applies when the SCVP operates with a neutral density filter and one set that applies when it operates without a neutral density filter.

Twelve expressions were obtained for brightness temperature versus grey level by solving for the lamp current as a function of grey level, using each one of the twelve relationships just mentioned, and by substituting the expression for lamp current into the relation for brightness temperature versus current at the appropriate wavelength. For each of these twelve relations an expression was obtained for the uncertainty in the brightness temperature as a function of grey level, which has the form below.

$$\sigma_T = \sqrt{\sigma_A^2 + \sigma_B^2 \frac{GL-C}{D} + 2\sigma_{AB}^2 \sqrt{\frac{GL-C}{D}} + \frac{B^2\left(\sigma_C^2 + \frac{\sigma_D^2}{D^2}\right)}{4D\,(GL-C)}}, \tag{8}$$

where σ_A, σ_B, σ_C, σ_D are the variances in the fitting parameters A, B, C and D, discussed previously. σ_{AB} is the covariance of the parameters A and B. GL denotes a grey level value as before. A sample of the results of the calibration is presented in Figures (7) and (8) for the case of the 660 nm with and without a neutral density filter.

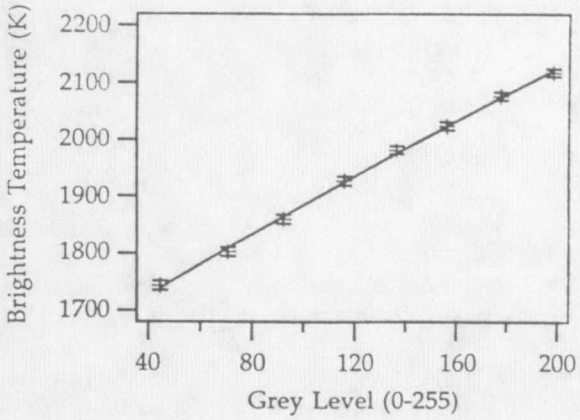

Figure 7: Brightness temperature at 660 nm vs. grey level without neutral density filter.

3.3 Sensitivity Range

The calibration described above effectively gives two possible "settings" for the sensitivity range of the SCVP. They are:

- RANGE I, extends from about 1750 °K to about 2150 °K
- RANGE II, covers temperatures roughly between 2150 °K and 2700 °K

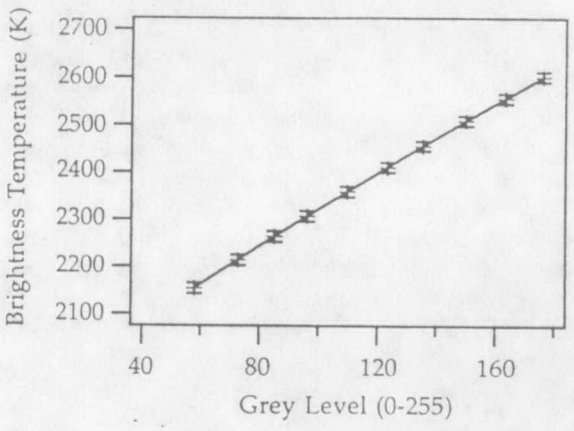

Figure 8: Brightness temperature at 600 nm vs. grey level with a neutral density filter.

Of course the SCVP can be calibrated to cover other ranges or wider ranges through a judicious choice of aperture and/or neutral density filter.

4 Data Reduction Algorithm

4.1 Algorithm for Estimating True Temperature

4.1.1 Formalism

The determination of the true temperature begins after the pixel grey level information about the surface is reduced to get the brightness temperature at each of the six wavelengths. To go from brightness temperature to true temperature we adopt the algorithm developed by Hoch[8] (1992) with a modification that allows the calibration errors in the brightness temperature to be carried in the multiple regression analysis described below.

Hoch[8] presents a sophisticated algorithm, briefly described below, that effectively compensates for the unknown form of the emissivity-wavelength relation (Eq. (3)) by repeating a multiple regression on a set of pyrometric equations (also described below) for various successive orders of the polynomial in Eq. (3). The errors associated with each of these regressions is used to weight the adequacy of the corresponding polynomial. He shows using published data that the method gives good accuracy. The interested reader is referred to that paper for more details.

In essence, for each of the six brightness temperatures an equation of the form of Eq. 1 can be written, producing a system of six equations with the temperature as one unknown. Eq. 3 is then substituted for $\ln \epsilon$. The maximum number of parameters, a_i that can be used with Eq. 3 is limited to five, because there are only six equations. This allows at most a fourth order polynomial approximation to $\ln \epsilon$. The temperature is eliminated from the system of equations by subtracting pairwise combinations of the six equations to obtain equations of the form

$$\left(\frac{1}{T_{Bj}} - \frac{1}{T_{Bi}}\right) = \frac{1}{c}\sum_{k}^{n} a_k \left(\lambda_i^{k+1} - \lambda_j^{k+1}\right). \qquad (9)$$

The number of terms in the summation depends on the degree of the polynomial used to approximate $\ln \epsilon$, and polynomials of different degrees are used in the analysis. There are fifteen equations of the form of Eq. 9, generated by subtracting each of the original six equations with each of the others, once. The problem of finding the true temperature is reduced to a problem where n parameters, a_k, above, are to be determined. A multiple regression analysis is applied to determine the parameters and the error associated with each parameter.

4.1.2 Multiple Regression

The 15 relations in Eq. (9) can be modeled as n (15) observations on a dependent response y and p (order of the polynomial) independent variables $x_1, x_2, x_3, \cdots, x_p$. The linear relationship in Eq. (9) can thus be modeled as

$$y_i = \beta_0 + \beta_1 x_{1i} - \beta_2 x_{2i} + \cdots + \beta_p x_{pi} + u_i \qquad (10)$$

where, y_i is the term on the left side of Eq. (9), the x values are $\beta_0, \beta_1, \beta_2, \cdots, \beta_p$ are called the model *partial regression coefficients* and represent the constants a_k, while u_i is a random disturbance.

The β's are estimated by minimizing the sum of squared residuals (method of least squares)

$$\begin{aligned} S(\beta_0, \beta_1, \beta_2, \cdots, \beta_p) &= \sum_{i=1}^{n} u_i^2 \qquad (11) \\ &= \sum_{i=1}^{n} (y_i - \beta_0, \beta_1 x_{1i}, \beta_2 x_{2i}, \cdots, \beta_p x_{pi})^2 \end{aligned}$$

From calculus it can be shown[16] that the lease square estimates $b_0, b_1, b_2, \cdots, b_p$ which minimize

$S(\beta_0, \beta_1, \beta_2, \cdots, \beta_p)$ are given by the solution of the following system

$$\begin{aligned} S_{11}b_1 + S_{12}b_2 + S_{13}b_3 + \cdots + S_{1p}b_p &= S_{y1} \quad (12) \\ S_{12}b_1 + S_{122}b_2 + S_{23}b_3 + \cdots + S_{2p}b_p &= S_{y2} \quad (13) \\ \vdots \qquad\qquad & \vdots \quad (14) \\ S_{1p}b_1 + S_{2p}b_2 + S_{3p}b_3 + \cdots + S_{pp}b_p &= S_{yp} \quad (15) \end{aligned}$$

where

$$S_{ij} = \sum_{k=1}^{n} (x_{ik} - \bar{x}_i)(x_{jk} - \bar{x}_j), \quad i, j = 1, 2, \cdots, p; \tag{16}$$

$$S_{yi} = \sum_{k=1}^{n} (y_k - \bar{y})(x_{ik} - \bar{x}_i), \quad i, j = 1, 2, \cdots, p; \tag{17}$$

$$\bar{x}_i = \frac{\sum_{k=1}^{n} x_{ik}}{n} \tag{18}$$

$$\bar{y} = \frac{\sum_{k=1}^{n} y_k}{n} \tag{19}$$

and

$$b_0 = \bar{y} - b_1\bar{x}_1 - b_2\bar{x}_2 - b_3\bar{x}_3 - \cdots - b_p\bar{x}_p. \tag{20}$$

Finally, we can calculate the variance σ_i associated with each estimate b_i from [16]

$$\sigma_i^2 = \frac{\sum_{i=1}^{n} (y_i - b_0 - b1x_{1i} - b2x_{2i} - \cdots - b_p x_{pi})^2}{n - p - 1} c_{ii} \tag{21}$$

where the c_{ii} are the diagonal elements of the covariance matrix C

$$C = (X^T X)^{-1} \tag{22}$$

and X is the matrix containing the values of the observations.

The actual method we used in our code is an extension of the above formalism that allows including also errors associated with the observations y_i as outlined in Ref. [15]. In our case these are errors calculated using the left side of Eq. (9) and the variances from Eq. (8).

4.1.3 Weighting Polynomial Form Contribution with Associated Errors

Once the n parameters are determined, they are substituted into the original six equations relating true temperature to brightness temperature and six values for temperature are obtained. An error propagation analysis is then used to get the uncertainty in each case. An average is taken from these values to represent the temperature, T_p, obtained when using a n^{th} degree polynomial to approximate $\ln \epsilon$. The steps above are repeated using different polynomial approximations where n ranges from 2 to 5 and four values for T_p are generated with their associated uncertainties. Values of T_p that are negative are discarded, because such T_p are physically meaningless and correspond to poor choices for the polynomial approximation of $\ln \epsilon$. A weighted average is taken of the acceptable T_p and this result is taken as the true temperature.

4.2 Digital Processing

The above calculations must be carried for each pixel of each of the six frames constituting a complete data set. This represents an intensive floating point calculation task for a computer. Vector coding techniques were used to speed the calculations. A stand-alone interactive computer program for SCVP data processing was developed. The program takes the raw pixel data from six consecutive video frames and provides, as output, false-color raster pictures of the true temperature and the associated errors, using the "hot metal" color palette as illustrated in the example of Section 5.

Finally, it is important to mention that the transmission line noise typical of common CCD cameras with analog output (and possibly CCD array stability) can cause random fluctuations in the pixel values on the order of 1 to 3 grey levels per pixel. This noise can adversely affect the analysis and cause large errors for the affected pixels. Luckily this problem can be quite effectively alleviated by applying to the raw data a digital noise filter commonly used in image processing. This filter, sometimes called "Median Filter"[17], replaces the value of each pixel by a value obtained from averaging the values of the surrounding pixels. A median filter of order 1 (i.e. averages only pixels that are 1 pixel away from the center pixel) was coded as an integral part of the SCVP software.

5 Experimental Results

The experiment reported in this section was conducted in EPPDyL's Steady-State Low Power (SSLP) Facility described in ref. [18]. The SSLP facility uses a 1.5 m diameter cylindrical carbon steel tank, 6.4 m in length, evacuated to 10^{-5} torr by a set of mechanical and diffusion pumps. The steady-state

MPD thruster and the associated subsystems are described in ref. [19]. For this experiment the thruster was operated at 200 A with 6 mg/s of argon propellant. The location and configuration of the SCVP is shown schematically in Fig. (5).

The SCVP was operated in the RANGE I sensitivity mode (i.e. no neutral density filters).

The output of the SCVP is shown in Fig. (9) along with the input frames. Panel (a) shows the pixel grey levels for the six video frames corresponding to the six filters of the pyrometer using a "hot metal" color palette. It can be noted that the grey level did not exceed 180.

Panel (b) of that figure shows the resulting SCVP output for the true temperature on the cathode which varies between 1750 and 2000 °K for the pixels shown. Only pixels whose true temperature error is below 10% are shown. From Panel (c) which shows the associated error, we note that the region of the cathode that is associated with large errors (above 10%) in the true temperature correspond to the cooler upstream part of the cathode whose temperature falls below the sensitivity range (1750 °K) of the SCVP. In other words, the blackest pixels in Panel (b) correspond to temperature below the sensitivity of the SCVP operating in RANGE I.

It is important to note that for most of the colored pixels resolved in Panel (b), the errors are lower than 5%. The data also indicates that an extension of the calibration curves to temperature (sensitivity) ranges lower (higher) than RANGE I is needed to resolve the rest of the cathode. This can be easily accomplished by recalibrating with a lower f-stop. This will not risk saturating the SCVP since there exists enough latitude above grey level 180 to allow for the increase in the sensitivity before saturation is reached.

6 Conclusions

A six-color video pyrometer (SCVP) that exploits the full potential of computer aided video analysis was developed for taking spatially resolved measurements of high temperature surfaces. The SCVP is most useful in situations where the emissivity is unknown, as in case of the lithium-fed MPD thruster. Critical design and implementation issues concerning the SCVP were discussed. A detailed description of the calibration and data reduction procedures was given. An example of the SCVP application was illustrated with temperature measurement of an MPD thruster cathode.

The instrument has a time resolution of 200 ms and an arbitrary spatial resolution proportional to the number of pixels over which the object is focused. With its present calibration it can accurately resolve temperatures ranging between 1750 and 2800 °K.

Acknowledgments The authors are thankful to Waldo von Jaskowsky, John Ziemer, Roger Chen, Paolo Gessini and Kingston Lam for their valuable contributions to this work.

References

[1] S. Krishnan. Calibration, properties, and applications of the division-of-amplitude photopolarimeter at 632.8 and 1523 nm. *Journal of the Optical Society of America A*, 9:1615–1622, 1992.

[2] H.J. Kostowski and G.W. Burns. Thermocouple and radiation thermometry above 900 ok. In *Measurements Techniques in Heat Transfer*. Technivision Series, Slough, UK, 1970.

[3] P.B. Coates. Multi-wavelength pyrometry. In *Metrologia, Vol. 17*. Springer Verlag, Berlin, 1981.

[4] R. Chen, E.Y. Choueiri, P. Gessini, K. Lam., D. Maneypanda, E. Schneider, and W. von Jaskowski. Lithium plasma thruster research. contributions to the Semi-Annual Progress Report for the period June 1994-December 1994. Technical Report No. EPPDyL-TR-94F, EPPDyL, Princeton University, 1994.

[5] D. Ya Svet. Determination of the emissivity of a substance from the spectrum of its thermal radiation and optimal methodes of optical pyrometry. *High Temperatures - High Pressures*, 8:493–498, 1976.

[6] J.L. Gradner, T.P. Jones, and M.R. Davies. A six-wavelength radiation pyrometer. In *High Temperatures, High Pressures, vol. 13*. Pion Limited, UK, 1981.

[7] J.P. Hiernaut, R. Beukers, Heinz W, R. Slefslag, M. Hoch, and R.W. Ohse. Submillisecond six-wavelength pyrometer for high temperature measurements in the range 2000 to 5000 ok. In *High Temperatures, High Pressures, vol. 18*. Pion Limited, UK, 1986.

[8] M. Hoch. The integral six-color pyrometer: a new general method of temeprature determination. *High Temperatures - High Pressures*, 24:607–623, 1992.

[9] J.S. Fillmore. Lithiated cathode plasma thruster research. Technical Report MAE 1776.39, Electric Propulsion and Plasma Dynamics Laboratory, Princeton University, September-October 1992.

[10] A.N. Zaidel, V.K. Prokof'ev, S.M. Raiskii, V.A. Slavnyi, and E.Ya. Shreider. *Tables of Spectral Lines*. Plenum Press, New York, 1970.

[11] W.F. Meggers, C.H. Corlis, and B.F. Scribner. *Tables of Spectral-Line Intensities*. US Department of Commerce, National Bureau of Standards, Washington, DC, 1975.

[12] P.B. Coates. The direct calculation of radiance temperature in photoelectric pyrometry. In *High Temperatures, High Pressures, vol. 11*. Pion Limited, UK, 1979.

[13] T. J. Quinn. *Temperature*. Academic Press Ltd, second edition, 1990.

[14] R. D. Larrabee. Spectral emissivity of tungsten. *Journal of the Optical Society of America*, 49:619–625, 1959.

[15] P.R. Bevington and D.K. Robinson. *Data Reduction and Error Analysis for the Physical Sciences*. McGraw-Hill Inc., New York, 1992.

[16] S. Chatterjee and B. Price. *Regression Analysis by Example*. John Wiley & Sons, Inc., New York, 1991.

[17] Adobe Corporation. *Adobe Photoshop 3.0, User Guide*. Adobe Systems Inc, Mountain Vie, CA, 1994.

[18] J.S. Fillmore. An experimental study of lithium dispenser cathodes in the MPD thruster. In 23^{rd} *International Electric Propulsion Conference*, Seattle, WA, USA, 1993. IEPC-93-196.

[19] T.M. Randolph, W.F. Von Jaskowsky, A. J. Kelly, and R. G. Jahn. Measurement of ionization levels in the interelectrode region of an MPD thruster. In 28^{th} *Joint Propulsion Conference*, Nashville, TN, 1992. AIAA-92-3460.

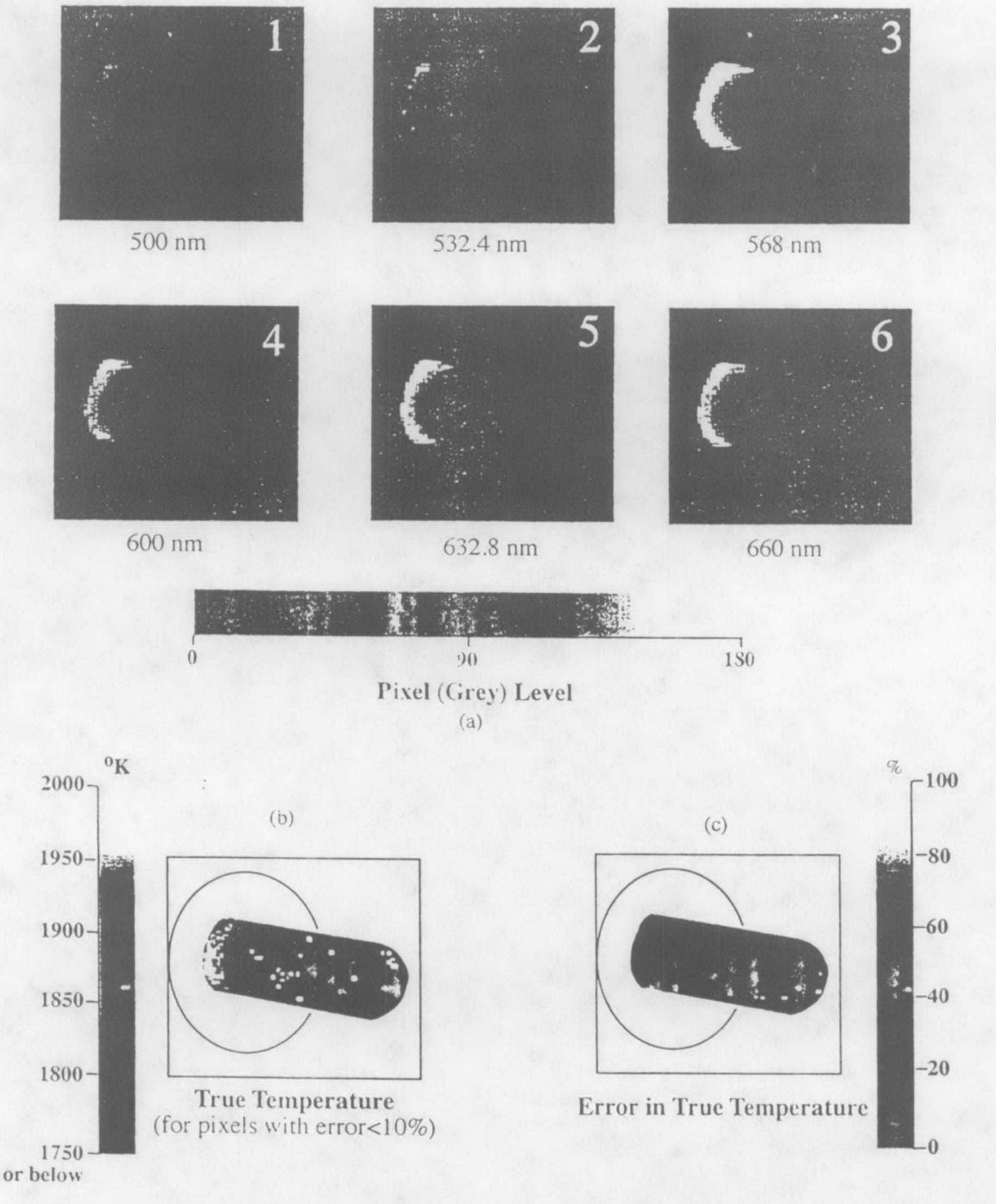

Figure 9: Panel (a) shows the pixel grey levels for the six video frames corresponding to the six filters of the pyrometer using a "hot metal" color palette. Panel (b) shows the true temperature on the cathode for pixels whose true temperature error is below 10%. Panel (c) shows the associated errors. Pyrometer range set at 1750-2200 °K.